# Investigation of thermally-induced phase mismatching in continuous-wave second harmonic generation: A theoretical model

**Mohammad Sabaeian,[1,*] Laleh Mousave,[2] and Hamid Nadgaran[3]**

[1] *Department of Physics, Faculty of Science, Shahid Chamran University of Ahvaz, Ahvaz, Iran*
[2]*Department of Physics, Islamic Azad University, Dezful Branch, Dezful, Iran*
[3]*Department of Physics, College of Science, University of Shiraz, Shiraz 71454, Iran*
[3]*nadgaran@susc.ac.ir*
**sabaeian@scu.ac.ir*

**Abstract:** A fraction of the fundamental beam energy deposited into nonlinear crystals to generate second harmonic waves (SHW) causes a temperature gradient within the crystal. This temperature inhomogeneity can alter the refractive index of the medium leading to a well-known effect called thermal dispersion. Therefore, the generated SHW suffers from thermal lensing and a longitudinal thermal phase mismatching. In this work by coupling the heat equation with second harmonic generation (SHG) formalism applied to type-II configuration along with walk-off effect, we investigate the continuous wave (CW) SHW beam profile and conversion efficiency when a non-linear KTP crystal is under induced thermal load. We have demonstrated for average and high powers, the thermal de-phasing lead to considerable reduction in SHG compared to an ideal case in which induced heat is neglected.



**OCIS codes:** (190.0190) Nonlinear optics; (140.6810) Thermal effects.

## References and links

1. M. Okada, and S. Ieiri, "Influence of self-induced thermal effects on second harmonic generation," IEEE J. Quantum Electron. **7**(9), 469–470 (1971).
2. J. D. Barry, and C. J. Kennedy, "Thermo-optical effects of intracavity $Ba_2Na(NbO_3)$ on a frequency-doubled Nd:YAG laser," IEEE J. Quantum Electron. **11**, 575–579 (1975).
3. D. T. Hon, "Electro-optical compensation for self-heating in CD*A during second-harmonic generation," IEEE J. Quantum Electron. **12**(2), 148–151 (1976).
4. D. T. Hon, and H. Bruesselabach, "Beam Shaping to Suppress Phase Mismatch in High Power Second-Harmonic Generation," IEEE J. Quantum Electron. **16**(12), 1356–1364 (1980).
5. E. Moses, H. Brusselbach, D. Stovall, and D. T. Hon, in *Proceeding of Soc. Opt. Quantum Electron. Conf. Lasers, Appl.,* (Orlando, FL. 1978).
6. D. Eimerl, "High Average Power Harmonic Generation," IEEE J. Quantum Electron. **23**(5), 575–592 (1987).
7. S. Seidel, and G. Mann, "Numerical modeling of thermal effects in nonlinear crystal for high power second harmonic generation," Proc. SPIE **2989**, 204–214 (1997).
8. J. Zheng, Sh. Zhao, Q. Wang, X. Zhang, and L. Chen, "Influence of thermal effect on KTP type-II phase-matching second-harmonic generation," Opt. Commun. **199**(1-4), 207–214 (2001).
9. M. E. Innocenzi, H. T. Yura, C. L. Fincher, and R. A. Fields, "Thermal modeling of continuous-wave end-pumped solid-state lasers," Appl. Phys. Lett. **56**(19), 1831–1833 (1990).
10. S. V. Tovstonog, S. Kurimura, I. Suzuki, K. Takeno, S. Moriwaki, N. Ohmae, N. Mio, and T. Katagai, "Thermal effects in high-power CW second harmonic generation in Mg-doped stoichiometric lithium tantalate," Opt. Express **16**(15), 11294–11299 (2008).
11. K. H. Hong, C. J. Lai, A. Siddiqui, and F. X. Kärtner, "130-W picosecond green laser based on a frequency-doubled hybrid cryogenic Yb:YAG amplifier," Opt. Express **17**(19), 16911–16919 (2009).
12. R. Peng, L. Guo, X. Zhang, F. Li, Q. Cui, Y. Bo, Q. Peng, D. Cui, Z. Xu, and L. Tang, "43 W picosecond laser and second-harmonic generation experiment," Opt. Commun. **282**(4), 611–613 (2009).
13. M. Sabaeian, and H. Nadgaran, "Bessel-Gauss beams: Investigation of thermal effects on their generation," Opt. Commun. **281**(4), 672–678 (2008).
14. Zh. Ren, Zh. Huang, S. Jia, Y. Ge, and J. Bai, "532 nm laser based on V-type doubly resonant intra-cavity frequency-doubling," Opt. Commun. **282**(2), 263–266 (2009).

#129028 - $15.00 USD Received 26 May 2010; revised 10 Jul 2010; accepted 11 Jul 2010; published 18 Aug 2010

15. Ch. Liu, Th. Riesbeck, X. Wang, J. Ge, Zh. Xiang, J. Chen, and H. J. Eichler, "Influence of spherical aberrations on the performance of dynamically stable resonators," Opt. Commun. **281**, 5222–5228 (2008).
16. J. D. Bierlein, and H. Vanherzeele, "Potassium titanyl phosphate: Properties and new applications," J. Opt. Soc. Am. B **6**(4), 622–633 (1989).
17. K. Asaumi, "Second-Harmonic Power of $KTiOPO_4$ with Double Refraction," Appl. Phys. B **54**(4), 265–270 (1992).
18. P. K. Mukhopadhyay, S. K. Sharma, K. Ranganthan, P. K. Gupta, and T. P. S. Nathan, "Efficient and high-power intracavity frequency doubled diode-side-pumped Nd:YAG/KTP continuous wave (CW) green laser," Opt. Commun. **259**(2), 805–811 (2006).
19. R. G. Smith, "Theory of intraccavity optical second harmonic generation," IEEE J. Quantum Electron. **6**(4), 215–223 (1970).
20. J. D. Barry, and C. J. Kennedly, "Thermooptical effects of intracavity $Ba_2Na(NbO_3)_5$ on a frequency doubling NdYAG laser," IEEE J. Quantum Electron. **11**, 575–579 (1975).
21. F. Q. Jia, Q. Zheng, Q. H. Xue, Y. K. Bu, and L. S. Qian, "High-power high-repetition-rate UV light at 355 nm generated by a diode-end-pumped passively Q-switched Nd:YAG laser," Appl. Opt. **46**(15), 2975–2979 (2007).
22. R. W. Boyd, *Nonlinear Optics,* 3rd ed. (Academic Press 2008), Chapt. 2.
23. J. A. Armstrong, N. Bloembergen, J. Ducuing, and P. S. Pershan, "Interaction between light waves in nonlinear medium," Phys. Rev. **127**(6), 1918–1939 (1962).
24. M. Sabaeian, H. Nadgaran, and L. Mousave, "Analytical solution of the heat equation in a longitudinally pumped cubic solid-state laser," Appl. Opt. **47**(13), 2317–2325 (2008).
25. K. Kato, "Parametric oscillation at 3.2 μm in KTP pumped at 1.064 μm," IEEE J. Quantum Electron. **27**(5), 1137–1140 (1991).
26. D. Zhang, J. Lu, B. Feng, and J. Zhang, "Increased temperature bandwith of second harmonic generator using two $KTiOPO_4$ crystals cut at different angles," Opt. Commun. **281**(10), 2918–2922 (2008).
27. Y. Bi, R. Li, Y. Feng, X. Lin, D. Cui, and Z. Xu, "Walk-off compensation of second harmonic generation in type-II phase-matched configuration with controled temperature," Opt. Commun. **218**(1-3), 183–187 (2003).

## 1. Introduction

Frequency conversion techniques are generally utilized in nonlinear optics to generate double and triple beam frequencies. In second harmonic generation (SHG), an optical wave of frequency ω is converted to a wave of 2ω. As activation of crystal nonlinear response needs crystal exposure to intense optical beams, one has to account for thermal effects suffered by the nonlinear crystal. These effects which are occurred through optical absorption of the fundamental wave (FW) and the second harmonic wave (SHW) by the medium should be extensively managed in most second harmonic generator devices. Among the most important thermal effects, other than thermal dispersion and induced thermal stress, one can name thermally-induced phase mismatching or in short thermal phase mismatching that plays a very crucial role in frequency conversion techniques. It can have severe impact on conversion efficiency and even can destroy phase matching to deny high intensity SHW.

Okada and Ieiri [1] solved a heat equation with various simplifying assumptions to account for SHG. Barry and Kendy [2] investigated the thermo-optics effect in $Ba_2Na(NbO_3)_5$ crystal to convert the Nd:YAG laser output. Others discussed different techniques, for instance, Hon tried to compensate self-heating, such as electro-optics effect [3], and beam shaping [4] to suppress thermal phase mismatching. Moses [5] worked on the so-called fanning and scanning in this respect. Eimerl [6] achieved high average power SHW by treating the nonlinear material as a set of thin plates letting the exposed surface be cooled with a flowing gas. He also proposed theoretical models for thermal de-phasing and thermal stress in SHG. Seidel and Mann [7] developed a numerical model including thermal phase mismatching for frequency doubling in KTP and compared their work with experimental. Zheng *et al.* [8] studied the effect of transverse thermal phase shift on type-II SHG in undepleted approximation. They used the analytical Innocenszi *et al.* [9] thermal model that does not address longitudinal temperature variation. In experimental side, we can name the work of Tovstonog *et al.* [10] in which they investigated the thermal behavior of single-pass SHG of CW green radiation in periodically poled Mg-doped stoichiometric lithium tantalite. Recently Hong *et al.* [11] have reported a thermal model in which they blame the temperature gradient inside a nonlinear crystal as the main limiting factor of the conversion efficiency. Thermal lensing has been also reported as the main responsible effect for beam quality degradation and beam profile deviation from a standard shape profile [12,13]. These effects can only be described when thermally-induced lens be taken into account [14,15]. Despite

#129028 - $15.00 USD Received 26 May 2010; revised 10 Jul 2010; accepted 11 Jul 2010; published 18 Aug 2010

very much excellent works in SHG with thermal effects considerations, in almost all works so far, the coupling of the two main equations of what we call heat and harmonics equations has not been performed. Therefore, to the best of our knowledge, a comprehensive and complete thermal model concerning SHG initiating from coupling of heat equation and harmonic generation formulation in which the absorption of fundamental and second harmonic waves are taken into account is missing in the literature.

$KTiOPO_4$ (KTP) is an excellent nonlinear crystal with high nonlinear conversion coefficient, wide allowable angle, small walking-off angle and relatively high damage threshold [16]. In type-II KTP phase matching configuration, the phase mismatching plays an important role, and the nonlinear conversion efficiency and SHW beam quality can be well affected by any de-phasing, a topic that this work is devoted to. For instance, phase matching can only be fulfilled at $\theta = 90^\circ$ and $\phi = 24.77^\circ$ for KTP when laser beam of 1064 nm wavelength is used for SHG where $\theta$ is the angle between ray propagation direction and the main axis of the crystal (Z), and $\phi$ is the angle between ray propagation direction and X axis in X-Y plane [17]. At these angles the effective nonlinear coefficient of the crystal has rather its maximum value whereas the beam walk-off effect remains at its minimum level, and therefore any dephasing can harm any pretuning at these angles.

Generally, SHWs are generated by two techniques [6]: intra-cavity doubling [18–20], in which the nonlinear crystal is placed inside the laser cavity and extra-cavity doubling, where the doubler is external to the cavity [21].

## 2. Method

In this paper, by working the case of extra-cavity doubling provided by KTP crystal, we have relaxed almost all approximations and simple assumptions to report a more complete model involving heat loads in SHG. Towards this aim we believe that the heat equation should be somehow coupled with SHG equations to simultaneously account for the extent of suffering of fundamental wave and SHW from induced heat. In this respect, the coupling has been accomplished through source term and thermal phase mismatching, that is in one hand the heat equation source includes fundamental and second harmonic wave powers and on the other the harmonic generation equations covers a mismatched thermal phase factor depending on transverse and longitudinal coordinates. In type-II phase matching two polarization components of the electric field of fundamental wave coincide orthogonal ordinary and extraordinary directions of the doubling crystal generating a field with polarization component along extraordinary direction [22]. Because of this, we apply the sum frequency rule with equal frequencies for fundamental waves. So, we will end up with five equations: a heat equation, a thermally mismatched phase integral and three equations pertaining to sum frequency generation rendering linear absorption [7] of fundamental and second harmonic waves consisting an exponential thermal phase. In heat equation treatment, a general case in which convection cooling mechanism for the two end faces and constant temperature condition for lateral faces were adopted. Throughout this work the walk-off effect is also taken into account.

### *2.1 Heat-Harmonic generation coupling*

In this section we construct the above mentioned coupled equations together with walk-off effect for the sake of generalization. Here we assume a 1064 nm fundamental wave is used to generate a 532nm SHW. Figure (1-a) shows the scheme of type-II phase matching for KTP crystals in which the polarization components of fundamental beam at frequency ω coincide orthogonal ordinary and extraordinary directions of crystal refractive index. Figure (1-b) shows the exit face of KTP crystal where the phase matched beam at frequency 2ω lies along extraordinary direction. Figure (1-c) shows the propagation directions of fundamental wave ($E_e^{\omega}$ and $E_o^{\omega}$) at wavelength of $\lambda_1 = 1064\,nm$ and SHW ($E_e^{2\omega}$) at $\lambda_2 = 532nm$. This figure

#129028 - $15.00 USD Received 26 May 2010; revised 10 Jul 2010; accepted 11 Jul 2010; published 18 Aug 2010

also shows the walk-off angles of $\rho_1 = 0.00290227$ rad, $\rho_2 = 0.00564084$ rad and $\rho_3 = 0.00273857$ rad [17].

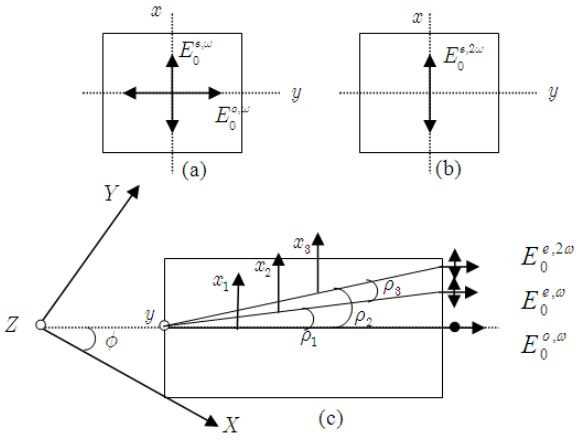


Fig. 1. (a) The entrance face of KTP crystal showing the coincidence of the two components of FW electric field to ordinary and extraordinary components of fundamental wave at frequency ω. (b) KTP exit face with extraordinary component of SHW at frequency 2ω. (c) The relation between crystallographic axes XYZ and optical beam axes xyz within XY crystallographic plane [17].

Using sum frequency rule and assuming plane wave for fundamental wave fields with a Gaussian transverse distribution, we can write the preliminary form of fields as [17,8]:

$$E^{o,\omega}(x,y,z) = E_0^{o,\omega} \exp\left[-\frac{(x+\rho_2 z)^2 + y^2}{\omega_F^2}\right], \tag{1}$$

$$E^{e,\omega}(x,y,z) = E_0^{e,\omega} \exp\left[-\frac{(x+\rho_3 z)^2 + y^2}{\omega_F^2}\right], \tag{2}$$

where $E_0^{o,\omega}$ and $E_0^{e,\omega}$ are amplitudes of fundamental wave and $\omega_F$ is their constant beam waist. Suppose at ambient temperature, the crystal is in a complete phased matched situation, the following system of equations can then describe the continuous wave sum frequency generation in MKS unit [22,23]:

$$\frac{dE^{o,\omega}}{dz} + \frac{\gamma_1}{2} E^{o,\omega} = \frac{2i\omega d_{eff}}{\varepsilon_0 n_o^{\omega} c} E^{e,2\omega} E^{*e,\omega}, \tag{3}$$

$$\frac{dE^{e,\omega}}{dz} + \frac{\gamma_2}{2} E^{e,\omega} = \frac{2i\omega d_{eff}}{\varepsilon_0 n_e^{\omega} c} E^{e,2\omega} E^{*o,\omega}, \tag{4}$$

$$\frac{dE^{e,2\omega}}{dz} + \frac{\gamma_3}{2} E^{e,2\omega} = \frac{4i\omega d_{eff}}{\varepsilon_0 n_e^{2\omega} c} E^{o,\omega} E^{e,\omega}, \tag{5}$$

with the following boundary conditions:

$$E_0^{o,\omega}(x,y,z=0) = \sqrt{2P^o c / n_o^{\omega} \varepsilon_0 \pi \omega_F^2}, \tag{6}$$

#129028 - $15.00 USD Received 26 May 2010; revised 10 Jul 2010; accepted 11 Jul 2010; published 18 Aug 2010

$$E_0^{e,\omega}(x,y,z=0)=\sqrt{2P^e c/n_e^{\omega}\varepsilon_0\pi\omega_F^2}, \tag{7}$$

$$E^{e,2\omega}(x,y,z=0)=0. \tag{8}$$

In above equations, $\gamma_1$ and $\gamma_2$ are the absorption coefficients of ordinary and extraordinary fundamental waves both at $1064nm$, $\gamma_3$ is the absorption coefficients of second harmonic wave at $532nm$, $d_{eff}$ is the effective nonlinear coefficient of KTP crystal, $\varepsilon_o$ is the vacuum permeability, $c$ is the speed of light, and $n_o^{\omega}$, $n_e^{\omega}$ and $n_e^{2\omega}$ are the refractive indices of ordinary wave at frequency $\omega$, extraordinary wave at frequency $\omega$ and extraordinary wave at frequency $2\omega$, respectively. $P^o$ and $P^e$ denote the initial power of ordinary and extraordinary waves at entrance face of the crystal, respectively letting $P^o=P^e=P$.

Let's investigate heat transfer equation here. The equation governing heat transfer in steady-state regime is given by [24]:

$$\nabla^2 T(x,y,z)=-S(x,y,z)/K, \tag{9}$$

where $T$ is temperature, $S$ is heat source density in W/m$^3$ and $K$ is thermal conductivity in W/m/K. The proper boundary conditions for six faces of the crystal are [24]:

$$-K\ \frac{\partial T(x,y,z)}{\partial z}\Big|_{z=0}=h\left[T(x,y,z=0)-T_0\right], \tag{10}$$

$$K\frac{\partial T(x,y,z)}{\partial z}\Big|_{z=c}=h\left[T(x,y,z=c)-T_0\right], \tag{11}$$

$$T(x=0,y,z)-T_0=T(x=a,y,z)-T_0=0, \tag{12}$$

$$T(x,y=0,z)-T_0=T(x,y=b,z)-T_0=0, \tag{13}$$

in which for end faces we used the convection condition and for lateral faces we used the constant temperature condition. In above equations h = 10 W/m$^2$/K is the heat transfer coefficient, $T_0=300K$ is the ambient temperature and $a$, $b$ and $c$ are the dimensions of crystal as $2\times2\times20\,mm^3$.

The source term can be written as $S=\gamma_1 I^{o,\omega}+\gamma_2 I^{e,\omega}+\gamma_3 I^{e,2\omega}$ where $I^{o,\omega}=n_o^{\omega}c\varepsilon_0\left|E^{o,\omega}\right|^2/2$, $I^{e,\omega}=n_e^{\omega}c\varepsilon_0\left|E^{e,\omega}\right|^2/2$ and $I^{e,2\omega}=n_e^{2\omega}c\varepsilon_0\left|E^{e,2\omega}\right|^2/2$ are the intensities of ordinary fundamental wave, extraordinary fundamental wave and second harmonic wave, respectively [8]. So, we conclude the source term by:

$$S=\frac{1}{2}c\varepsilon_0\left[\gamma_1 n_o^{\omega}\left|E_0^{o,\omega}\right|^2 e^{-2[(x+\rho_2 z)^2+y^2]/\omega_F^2}+\gamma_2 n_e^{\omega}\left|E_0^{e,\omega}\right|^2 e^{-2[(x+\rho_3 z)^2+y^2]/\omega_F^2}+\gamma_3 n_e^{2\omega}\left|E^{e,2\omega}\right|^2\right]. \tag{14}$$

The above expression shows our first heat-harmonic coupling equation in which the electric field of fundamental wave is explicitly coupled to the source term.

On the other hand, we have allowed the variation of the principle refractive indices of KTP crystal against temperature through Sellmeier equations by [25]:

$$n_x^2(\lambda,T_0)=3.0065+\frac{0.03901}{\lambda^2-0.04251}-0.01327\lambda^2, \tag{15}$$

$$n_y^2(\lambda,T_0)=3.0333+\frac{0.04154}{\lambda^2-0.04547}-0.01408\lambda^2, \tag{16}$$

#129028 - $15.00 USD Received 26 May 2010; revised 10 Jul 2010; accepted 11 Jul 2010; published 18 Aug 2010

$$n_z^2(\lambda,T_0)=3.3134+\frac{0.05694}{\lambda^2-0.05658}-0.01682\lambda^2, \tag{17}$$

where $\lambda$ is wavelength in $\mu m$. At temperature T, the refractive indices can be calculated by the following relations [26]:

$$n_x(\lambda,T)=n_x(\lambda,T_0)+\frac{dn_x}{dT}(T-T_0), \tag{18}$$

$$n_y(\lambda,T)=n_y(\lambda,T_0)+\frac{dn_y}{dT}(T-T_0), \tag{19}$$

$$n_z(\lambda,T)=n_z(\lambda,T_0)+\frac{dn_z}{dT}(T-T_0), \tag{20}$$

where the temperature derivatives of principal indices of KTP can be given as [27]:

$$\frac{dn_x}{dT}=(0.1323\lambda^{-3}-0.4385\lambda^{-2}+1.2307\lambda^{-1}+0.7709)\times10^{-5}(^\circ C^{-1}), \tag{21}$$

$$\frac{dn_y}{dT}=(0.5014\lambda^{-3}-2.0030\lambda^{-2}+3.3016\lambda^{-1}+0.7498)\times10^{-5}(^\circ C^{-1}), \tag{22}$$

$$\frac{dn_z}{dT}=(0.3896\lambda^{-3}-1.3332\lambda^{-2}+2.2762\lambda^{-1}+2.1151)\times10^{-5}(^\circ C^{-1}). \tag{23}$$

The relation between principal refractive indices ($n_x$, $n_y$ and $n_z$) and ordinary and extraordinary refractive indices ($n_o$ and $n_e$) to be used in Eqs. (3) to (5) at 1064 and $523\,nm$ is given by [27]:

$$n=\frac{\sqrt{2}}{\sqrt{-B\pm\sqrt{B^2-4C}}}, \tag{24}$$

where "+" and "−" signs correspond to the refractive indices of fast and slow light in the crystal, respectively and [27]:

$$B=-\sin^2\theta\cos^2\phi(b+c)-\sin^2\theta\sin^2\phi(a+c)-\cos^2\theta(a+b), \tag{25}$$

$$C=\sin^2\theta\cos^2\phi\ bc+\sin^2\theta\sin^2\phi\ ac+\cos^2\theta\ ab, \tag{26}$$

$$a=n_x^{-2},\ b=n_y^{-2},\ c=n_z^{-2}. \tag{27}$$

By using Eqs. (18)-(20), we first calculate the principal refractive indices at temperature $T$, then convert them to $n_o$ and $n_e$ via Eq. (24), with $\phi=24.77^\circ$ and $\theta=90^\circ$ [17].

The thermal phase mismatching due to temperature change of crystal can be written as [26]:

$$\Delta\Phi=\frac{2\pi}{\lambda_1}\int_0^z\left[n_e^{\omega}(T)-n_e^{\omega}(T_0)\right]dz+\frac{2\pi}{\lambda_1}\int_0^z\left[n_o^{\omega}(T)-n_o^{\omega}(T_0)\right]dz-\frac{2\pi}{\lambda_2}\int_0^z\left[n_e^{2\omega}(T)-n_e^{2\omega}(T_0)\right]dz, \tag{28}$$

where $\lambda_1$ and $\lambda_2$ stand for pump wavelength and second harmonic wavelength, respectively.

To consider the role of thermal effects in SHG formalism, it is time to include thermal phase mismatching in addition to temperature-dependent refractive indices. Therefore, the

#129028 - $15.00 USD Received 26 May 2010; revised 10 Jul 2010; accepted 11 Jul 2010; published 18 Aug 2010

terms $\exp(-i\Delta\Phi)$ should also be multiplied to the right hand side of Eqs. (3) and (4), and $\exp(i\Delta\Phi)$ to the right hand side of Eq. (5).

Finally, we ended up with five equations to be solved simultaneously to address the effect of heat load, i.e. Equations (3), (4) and (5) together with Eqs. (9) and (28).

The following dimensionless quantities do simplify the relations already introduced:

$$\psi_1 = \sqrt{\frac{I^{o,\omega}(x,y,z)}{I_0^{o,\omega}(x,y,z=0)}} = \frac{E_0^{o,\omega}(x,y,z)}{\sqrt{2P/n_o^{\omega} c\varepsilon_0 \pi \omega_F^2}}, \tag{29}$$

$$\psi_2 = \sqrt{\frac{I^{e,\omega}(x,y,z)}{I_0^{e,\omega}(x,y,z=0)}} = \frac{E_0^{e,\omega}(x,y,z)}{\sqrt{2P/n_e^{\omega} c\varepsilon_0 \pi \omega_F^2}}, \tag{30}$$

$$\psi_3 = \sqrt{\frac{I^{e,2\omega}(x,y,z)}{2I_0^{o(e)}(x,y,z=0)}} = \frac{E^{e,2\omega}(x,y,z)}{\sqrt{4P/n_e^{2\omega} c\varepsilon_0 \pi \omega_F^2}}. \tag{31}$$

The quantities $\eta_1 = |\psi_1|^2 e^{-2\left[(x+\rho_2 z)^2+y^2\right]/\omega_F^2}$ and $\eta_2 = |\psi_2|^2 e^{-2\left[(x+\rho_3 z)^2+y^2\right]/\omega_F^2}$ are clearly the efficiencies of fundamental wave components, and $\eta_3 = |\psi_3|^2$ is that of the SHW. To summarize, we can substitute Eqs. (29)-(31) into (3), (4), (5) and (9), to get our five genuine coupled equations as:

$$\frac{d\psi_1}{dz} + \psi_1\left[\frac{\gamma_1}{2} - 2\rho_2\frac{(x+\rho_2 z)}{\omega_F^2}\right] = \frac{\sqrt{2}}{\sqrt{n_1 n_2 n_3}}\frac{i}{l}\psi_3\psi_2^* e^{\left[(x+\rho_2 z)^2+y^2\right]/\omega_F^2} e^{-\left[(x+\rho_3 z)^2+y^2\right]/\omega_F^2} e^{-i\Delta\Phi}, \tag{32}$$

$$\frac{d\psi_2}{dz} + \psi_2\left[\frac{\gamma_2}{2} - 2\rho_3\frac{(x+\rho_3 z)}{\omega_F^2}\right] = \frac{\sqrt{2}}{\sqrt{n_1 n_2 n_3}}\frac{i}{l}\psi_3\psi_1^* e^{-\left[(x+\rho_2 z)^2+y^2\right]/\omega_F^2} e^{\left[(x+\rho_3 z)^2+y^2\right]/\omega_F^2} e^{-i\Delta\Phi}, \tag{33}$$

$$\frac{d\psi_3}{dz} + \frac{\gamma_3}{2}\psi_3 = \frac{\sqrt{2}}{\sqrt{n_1 n_2 n_3}}\frac{i}{l}\psi_1\psi_2 e^{-\left[(x+\rho_2 z)^2+y^2\right]/\omega_F^2} e^{-\left[(x+\rho_3 z)^2+y^2\right]/\omega_F^2} e^{i\Delta\Phi}, \tag{34}$$

$$\frac{d^2T}{dx^2} + \frac{d^2T}{dy^2} + \frac{d^2T}{dz^2} = -\frac{P}{\pi\omega_F^2 K}\left(\gamma_1|\psi_1|^2 e^{-2\left[(x+\rho_2 z)^2+y^2\right]/\omega_F^2} + \gamma_2|\psi_2|^2 e^{-2\left[(x+\rho_3 z)^2+y^2\right]/\omega_F^2} + \gamma_3|\psi_3|^2\right), \tag{35}$$

$$\Delta\Phi = \frac{2\pi}{\lambda_1}\int_0^z \left[\Delta n_1(T) + \Delta n_2(T) - 2\Delta n_3(T)\right]dz, \tag{36}$$

with boundary conditions of $\psi_1(z=0) = \psi_2(z=0) = 1$ and $\psi_3(z=0) = 0$. In the above equations $n_1$, $n_2$ and $n_3$ stand for $n_o^{\omega}$, $n_e^{\omega}$ and $n_e^{2\omega}$, respectively and $\Delta n_{1,2,3}(T) = n(T)_{1,2,3} - n(T_0)_{1,2,3}$. $l$ is also defined as $l = \sqrt{\varepsilon_0^3 c^3 \pi \omega_F^2 / 8\omega^2 d_{eff}^2 P}$.

## 3. Results and Discussions

To obtain simultaneous solutions of coupled Eqs. (32)-(36), we adopted finite difference method (FDM) in a home-made code programmed in MATLAB. The crystal was divided into 170 × 170 × 90 meshes to insure good convergence and reasonable CPU time. The thermal conductivity of KTP crystal is 13 W/m/K and its absorption coefficient at 1064nm is 10 $m^{-1}$ and at 532nm is 100 $m^{-1}$ [7]. The effective nonlinear coefficient of KTP is also 7.3$\varepsilon_0$ pm/V

#129028 - $15.00 USD Received 26 May 2010; revised 10 Jul 2010; accepted 11 Jul 2010; published 18 Aug 2010

and its ordinary and extraordinary refractive indices are $n_o^{\omega} = 1.8296$, $n_e^{\omega} = 1.7466$ and $n_e^{2\omega} = 1.7881$ [17].

*3.1 Thermal phase mismatching*

The first quantity that is more interested in this type of research is thermal phase mismatching induced by heat load. Figure (2-a) and (2-b) shows this thermal phase mismatching along x direction for Z = c/2 (c is the crystal length), y = 0 and for different input pump powers and pump spot size of $\omega_F$ = 0.2 mm and 0.3mm, respectively. The figure clearly shows that at low pump power, the amount of the thermal phase mismatching is rather small, whereas it increases considerably when the crystal is irradiated by more powerful pumps.

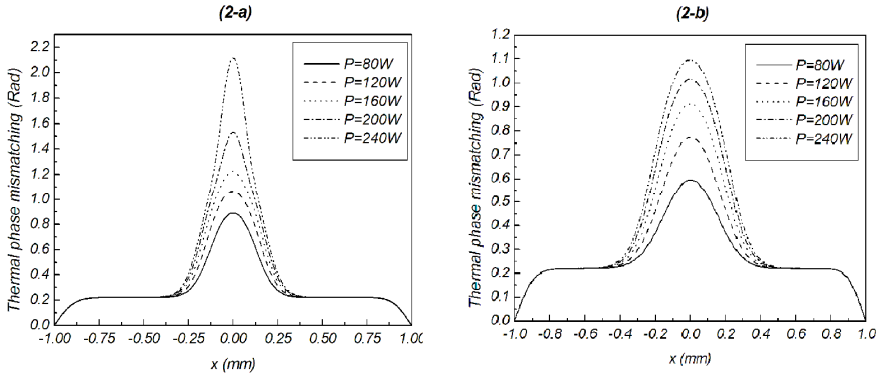


Fig. 2. The thermal phase mismatching versus x at y = 0 and z = c/2 for $\omega_F$ = 0.2 mm (a) and $\omega_F$ = 0.3 mm (b).

Comparison between Figs. (2-a) and (2-b) shows that when we use small spot sizes, the phase mismatching increases rapidly. In Fig. (2-a) for $\omega_F$ = 0.2mm this quantity for P = 240W is nearly 2.2 rad (in the midle of the crystal) whereas in Fig. (2-b) for $\omega_F$ = 0.3mm is halved. Figures (3-a)-(3-c) can be very useful in addressing the serious impact of induced heat on SHG. The figures show phase mismatching increase by increasing pump power along z-axis of the crystal. What we can extract from the these figures is that not only the induced thermal load is a serious matter in the SHG systems, particularly for average and high input powers and small spot size, but also its magnitude is not that negligible so that a sophisticated cooling mechanism must be designed to expect considerable efficiency for SHG.

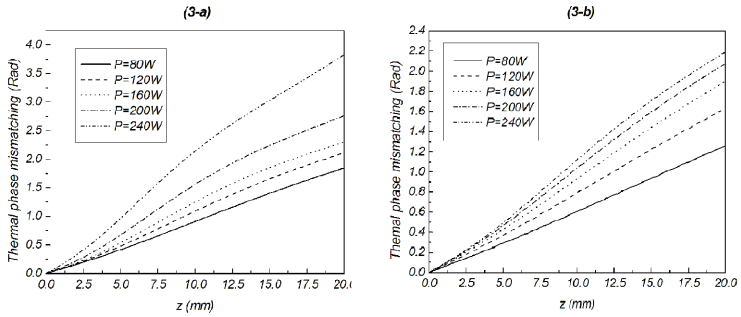


Fig. 3. The thermal phase mismatching versus z along the crystal axis (x = 0, y = 0) for $\omega_F$ = 0.1 mm (a), $\omega_F$ = 0.2 mm (b) and $\omega_F$ = = 0.2 mm (c) for various powers of fundamental wave.

#129028 - $15.00 USD Received 26 May 2010; revised 10 Jul 2010; accepted 11 Jul 2010; published 18 Aug 2010

*3-2 Efficiency*

High magnitude thermal phase mismatching imposes its manifestation on the SHG efficiency. This point is shown in Figs. (4-a)-(4-c) in which the variation of SHW efficiency, $\eta_3$, versus z along the crystal axis (x = 0 and y = 0) for various $\omega_F$ and total powers of fundamental waves $P = P^o + P^e$ are depicted. We compare these figures with that of non-thermal case, Fig. (4-d), to highlight the effects of thermal load, and to point out that the maximum efficiency for thermal case reaches about 57% for $\omega_F$ = 0.1 mm whereas this value would be almost 100% for non-thermal case. For small spot sizes, the efficiency tends to revive in shorter lengths, severely (Fig. 4-a). Close attention to these figures, reveals that for small spot sizes we can obtain higher efficiencies. The variation of the maximum efficiency against the input power is investigated more in Fig. (5-a).

These figures are clear in showing that higher pump powers leads to more revive the peaks of the efficiency and shift the location of the first maximum efficiency peak toward the head of the crystal; in fact the interaction length is reduced by increasing the input pump power.

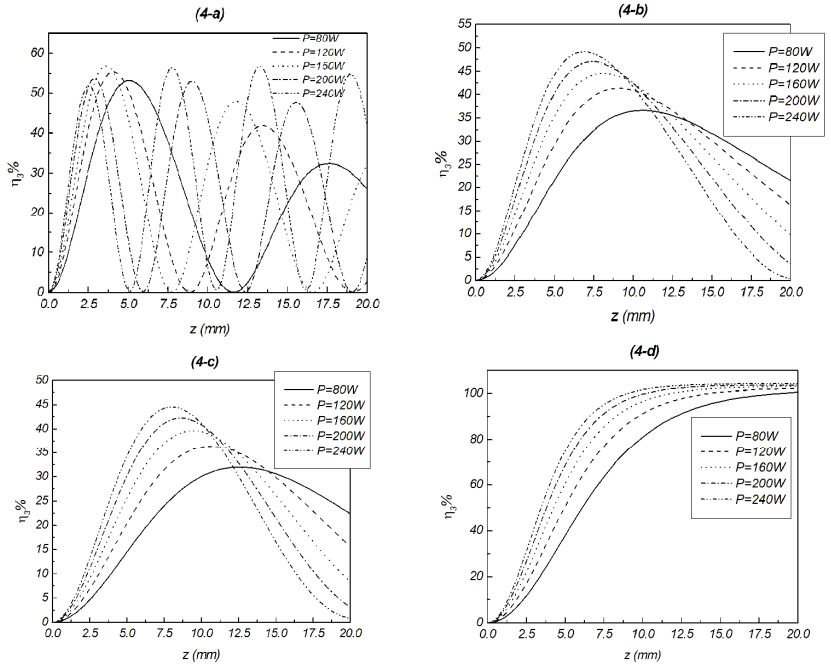


Fig. 4. Variation of $\eta_3$ versus z for $\omega_F$ = 0.1mm (a), $\omega_F$ = 0.2mm (b) and $\omega_F$ = 0.3mm (c) when thermal effects exist for various powers of fundamental wave. Efficiency of SHG for $\omega_F$ = 0.2mm for non-thermal case (d).

As figures show, one is pumping more power dense when employing smaller $\omega_F$ to achieve acceptable efficiency.

Comparison between Figs. (4-a) to (4-c) with that of experiments by Seidel and Mann [7] shows a good agreement in achieving considerable SHG efficiency.

In summary one can conclude this part of the article that the thermal effects are even more influential in generating SHW than in a simple solid-state laser so that various experimental parameters like the values of pump spot size, pump power, crystal length, etc should be somehow compromised to avoid severe thermal mismatching. The above conclusions can also be drawn when we consider the SHG efficiency at exit face of the crystal that is more interested by experimentalists.

To have a better insight to the effect of beam spot size on SHW efficiency, we plotted in Figs. (5-a) and (5-b) the maximum SHW efficiency versus input power for three values of

#129028 - $15.00 USD Received 26 May 2010; revised 10 Jul 2010; accepted 11 Jul 2010; published 18 Aug 2010

spot sizes, thermal and non-thermal cases, respectively. For $\omega_F$ = 0.1mm the higher efficiency is seen with some oscillations compared to $\omega_F$ = 0.2mm and $\omega_F$ = 0.3mm where show a smooth curve with smaller efficiencies. Our calculations show that for each spot size, the efficiency reaches to maxima for some specified input powers and then falls. The oscillatory behavior of efficiency becomes sever for smaller spot size. However, for non-thermal case, the efficiency reaches to a asymptotic value, i.e. to nearly 100% .

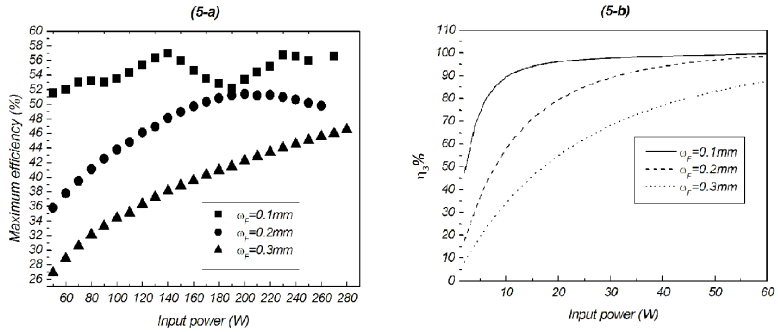


Fig. 5. The maximum efficiency of SHG ($\eta_3$) versus the total input power for three fundamental beam spot sizes for thermal case (a) and non-thermal case (b).

One other aspects of the thermal phase mismatching is its very clear impact on the generated beam profile. Comparing Figs. (6-a) to (6-c) with Fig. (6-d), at the exit face of the crystal, points out that induced thermal loads can have unsatisfactory effect on the SHW

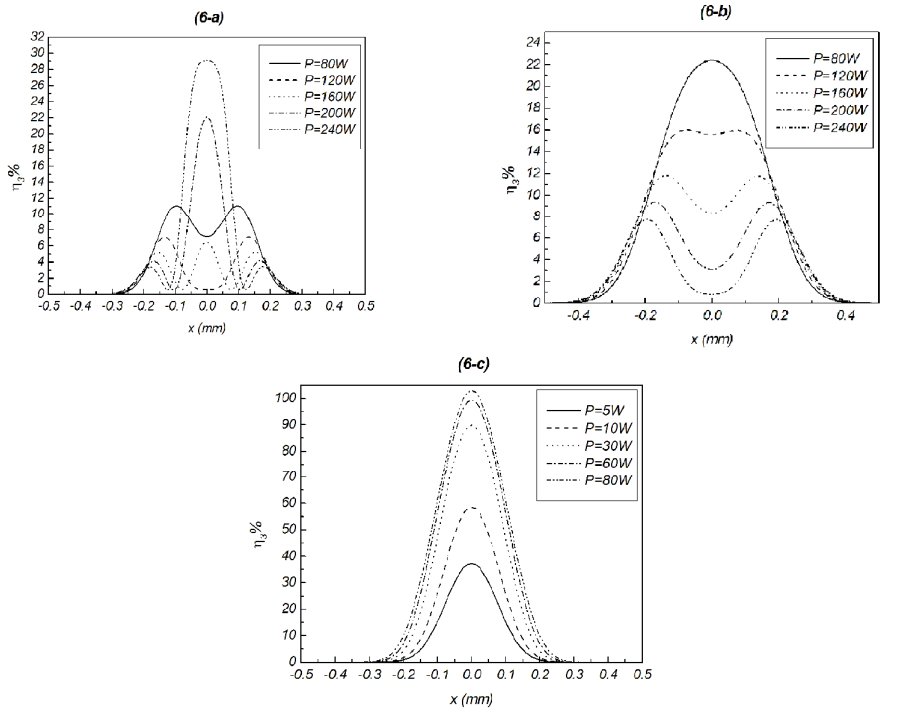


Fig. 6. The profiles of $\eta_3$ at the exit face of the crystal versus x for thermal case for $\omega_F$ = 0.2mm (a), $\omega_F$ = 0.3mm (b) and for non-thermal case for $\omega_F$ = 0.2mm (c) for various total fundamental powers.

#129028 - $15.00 USD Received 26 May 2010; revised 10 Jul 2010; accepted 11 Jul 2010; published 18 Aug 2010

profile emphasizing the importance of thermal loads in destroying an initial full phase matched set-up leading to strong de-phasing. This comparison is reporting that how a standard Gaussian profile of SHW in non-thermal case is destroyed by induced thermal load.

*3-3 Temperature distribution*

A glance at temperature change distribution of the crystal along x at z = c/2 and y = 0, Figs. (7), reveals that variation of temperature reaches such a value that can be very influential on initial tuned phase leading to low system performance caused by disturbing thermal phase mismatching. The width of the curves in Fig. (7) is increasing by pump spot size increase.

Figures (8-a) and (8-b) shows the temperature distribution along the z axis (x = 0, y = 0) for $\omega_F$ = 0.2mm and $\omega_F$ = 0.3mm, respectively. In Figs. (8) we see that from the head of the crystal to the point that the SHW efficiency has its way towards maximum efficiency, i.e. from 0 to nearly 7 mm in Fig. (4-b) and (4-c), the temperature increase shows a positive gradient. This is well attributed to the absorption of SHW that is one-order of magnitude larger than that of fundamental wave and therefore generates an appreciable amount of heat. This effect is also observed by Seidel and Mann [7]. As the second harmonic efficiency decreases, the heat load then decreases and in turn leads to lower temperatures and therefore a negative gradient.

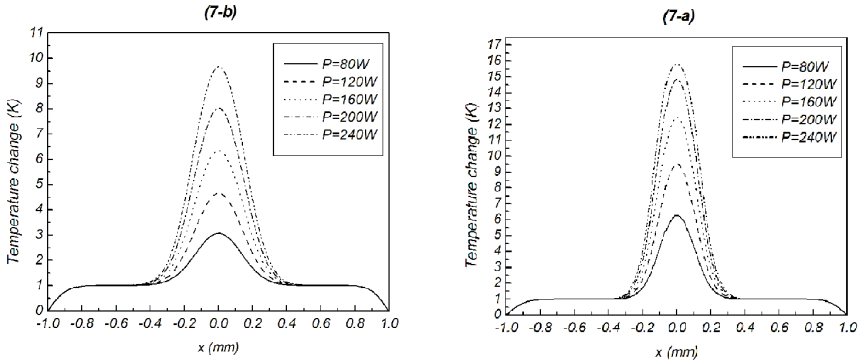


Fig. 7. Profiles of temperature change along x at y = 0 and z = c/2 for $\omega_F$ = 0.2mm (a), $\omega_F$ = 0.3mm (b).

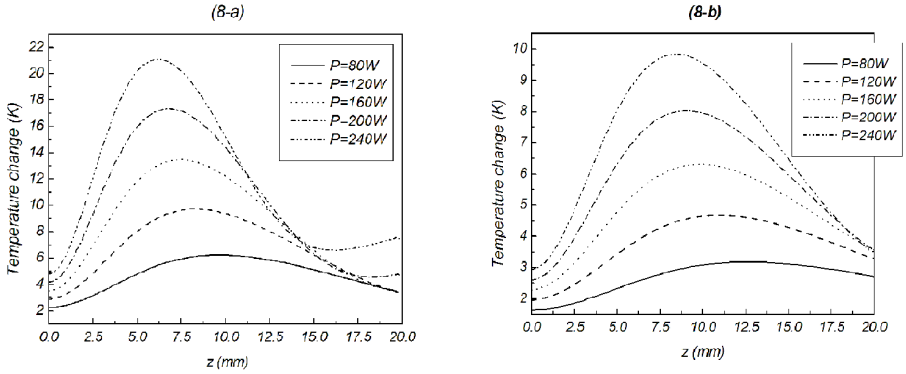


Fig. 8. Temperature change versus z along the crystal axis (x = 0 and y = 0) for $\omega_F$ = 0.2mm (a), $\omega_F$ = 0.3mm (b) for various fundamental powers.

## 4. Conclusion

Although the significance of the impacts of thermal effects on various laser and second harmonic generators' performances had been recognized since the laser invention era, because

#129028 - $15.00 USD Received 26 May 2010; revised 10 Jul 2010; accepted 11 Jul 2010; published 18 Aug 2010

of researchers' access to high power lasers, its importance has recently become the central part of laser system designs and constructions so that much works have been devoted to this both experimentally and theoretically. This paper tries to construct a better, realistic and reliable frame for this detrimental effect by relaxing the conventional approximations and simplifications in theoretical investigations of second harmonic generators.

For this purpose we have coupled the heat equation with second harmonic generation (SHG) formalism through thermally-induced phase mismatching or in short thermal phase mismatching including walk-off effect. Toward this we derived five coupled equations that properly describe the type-II harmonic generation. In this formalism, absorption of second harmonic and pump waves with Gaussian profile by a KTP crystal was investigated. In seeking the simultaneous solutions for our coupled equations, almost all approximations and simplifications already adopted by other researchers were relaxed. We have shown how the conversion efficiency of second harmonic waves (SHW) is influenced by induced heat. In this regard the thermal phase mismatching occurrence in denying satisfactory efficiency and standard beam profile was fully addressed. That is with thermally induced phase mismatching, the SHW beam profiles considerably deviates from a standard Gaussian shape despite the smallness of walk-off angles. Having reported the influential behavior of induced heat on SHG performance both quantitatively and qualitatively, we are in a position to announce that for better conversion efficiency and better SHW beam quality, the only limiting factor is not low quality non-linear crystal, but sound managing of the induced heat by employing proper heat removal mechanisms and in the same time avoiding disturbing temperature gradient play very essential role in SHW generators and in this way expensive high quality, large non-linear parameter crystal can only enhance the system performance at a mediocre level. This work not only propose a set of coupled equations and its solution, but also can be very useful for system designers to get realistic approach to better understanding of induced heat in intermediate power second harmonic generators.

#129028 - $15.00 USD Received 26 May 2010; revised 10 Jul 2010; accepted 11 Jul 2010; published 18 Aug 2010